The Norma cluster (ACO 3627) – I. A dynamical analysis of the most massive cluster in the Great Attractor

P. A. Woudt,[1]⋆ R. C. Kraan-Korteweg,[1] J. Lucey,[2] A. P. Fairall[1] and S. A. W. Moore[2]

[1]*Department of Astronomy, University of Cape Town, Private Bag X3, Rondebosch 7701, South Africa*
[2]*Department of Physics, University of Durham, Durham DH1 3LE*

ABSTRACT

A detailed dynamical analysis of the nearby rich Norma cluster (ACO 3627) is presented. From radial velocities of 296 cluster members, we find a mean velocity of $4871 \pm 54 \, \mathrm{km \, s^{-1}}$ and a velocity dispersion of $925 \, \mathrm{km \, s^{-1}}$. The mean velocity of the E/S0 population ($4979 \pm 85 \, \mathrm{km \, s^{-1}}$) is offset with respect to that of the S/Irr population ($4812 \pm 70 \, \mathrm{km \, s^{-1}}$) by $\Delta v = 164 \, \mathrm{km \, s^{-1}}$ in the cluster rest frame. This offset increases towards the core of the cluster. The E/S0 population is free of any detectable substructure and appears relaxed. Its shape is clearly elongated with a position angle that is aligned along the dominant large-scale structures in this region, the so-called Norma wall. The central cD galaxy has a very large peculiar velocity of $561 \, \mathrm{km \, s^{-1}}$ which is most probably related to an ongoing merger at the core of the cluster. The spiral/irregular galaxies reveal a large amount of substructure; two dynamically distinct subgroups within the overall spiral population have been identified, located along the Norma wall elongation. The dynamical mass of the Norma cluster within its Abell radius is $1–1.1 \times 10^{15} \, h_{73}^{-1} \, \mathrm{M_{\odot}}$. One of the cluster members, the spiral galaxy WKK 6176 which recently was observed to have a 70 kpc X-ray tail, reveals numerous striking low-brightness filaments pointing away from the cluster centre suggesting strong interaction with the intracluster medium.

Key words: galaxies: clusters: individual: Norma cluster (ACO 3627) – galaxies: elliptical and lenticular, cD – galaxies: individual: WKK 6176 – galaxies: kinematics and dynamics.

1 INTRODUCTION

The observed velocity flow field of galaxies in the nearby Universe is largely dominated by the Great Attractor (GA; Dressler et al. 1987; Lynden-Bell et al. 1988; Tonry et al. 2000) and the ∼3 times more distant Shapley supercluster (SCL) (Hudson et al. 2004). Both are extended overdensities in the large-scale mass distribution of the local Universe and both are thought to contribute significantly to the peculiar motion of the Local Group (LG) (Lucey, Radburn-Smith & Hudson 2005; Kocevski & Ebeling 2006). The relative contribution of the GA and the SCL to the motion of the LG, however, remains poorly determined (cf. Erdoğdu et al. 2006; Kocevski & Ebeling 2006) and is still a matter of debate.

The Shapley SCL is clearly visible as an overdensity in the distribution of Abell clusters (Scaramella et al. 1989; Einasto et al. 1997; Proust et al. 2006), whereas the GA and its location was identified first and foremost from the systematic peculiar velocities of galaxies streaming towards this apex (e.g. Lynden-Bell et al. 1988), and confirmed later from reconstructed mass-density fields of the local Universe (Dekel 1994; Kolatt et al. 1995; Erdoğdu et al. 2006).

However, no significant overdensity was obvious in the distribution of galaxies or Abell clusters at the position of the GA (Lynden-Bell & Lahav 1988). This is not surprising given the location of the GA with respect to the zone of avoidance (ZOA). Kolatt et al. (1995) locate the approximate centre of the extended GA overdensity at $(\ell, b, v) \sim (320°, 0°, 4000 \, \mathrm{km \, s^{-1}})$ based on their smoothed reconstructed mass-density field. The uncertainty in this position is ∼17° as a result of the applied smoothing of $1200 \, \mathrm{km \, s^{-1}}$; this smoothing is necessary given the sparsely sampled data (Kolatt et al. 1995). Towards such low Galactic latitudes, the view of the extragalactic light distribution is increasingly reduced by the dust and stars in the Milky Way. As a result, a large part of the GA overdensity is hidden from view by the Milky Way and early attempts to quantify the nature and extent of the GA (e.g. Dressler 1988; Jahoda & Mushotzky 1989; Rowan-Robinson et al. 1990; Hudson 1993a,b) were unsatisfactory: the clear (and significant) mismatch between the inferred mass of the GA and the visible galaxy distribution could not be understood.

A deep optical galaxy search at low Galactic latitudes in the GA region (Woudt & Kraan-Korteweg 2001) has lifted part of the veil of the Milky Way. Close to the predicted centre of the GA, the Norma cluster (ACO 3627: Abell, Corwin & Olowin 1989) has been identified as the most massive cluster in the GA region (Kraan-Korteweg
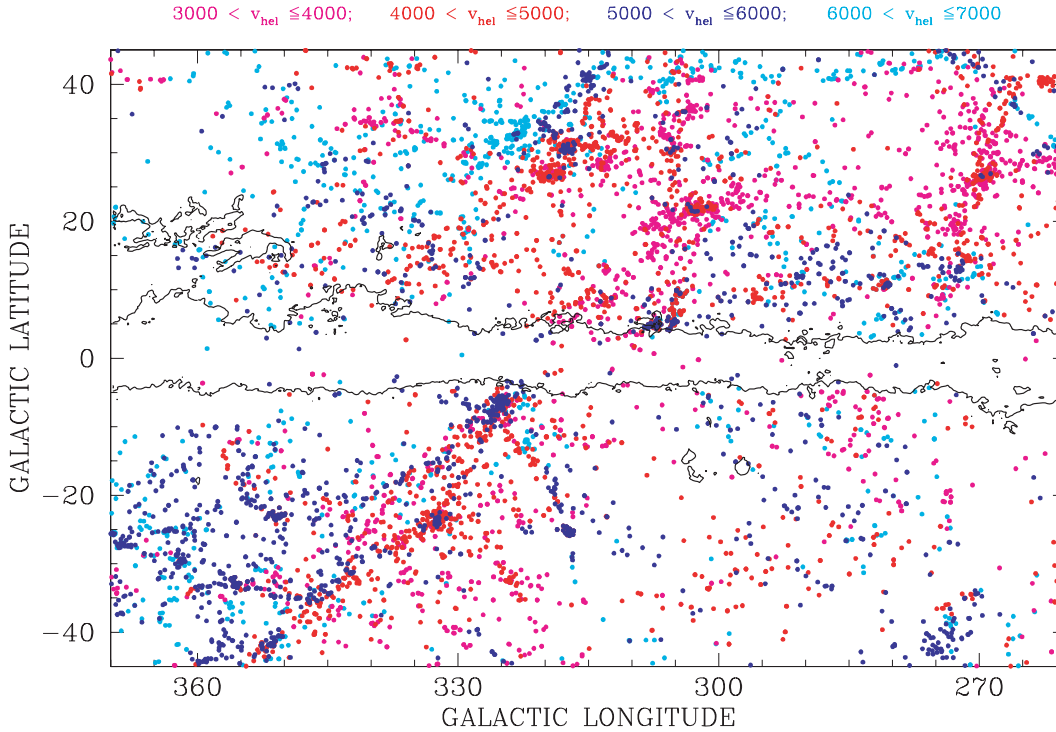
⋆E-mail: patrick.woudt@uct.ac.za

Figure 1. An overview of the large-scale structures in the GA region between $3000 < v_{hel} < 7000\,\mathrm{km\,s^{-1}}$. The Norma cluster is located at $(\ell, b, v) = (325°\!.3, -7°\!.2, 4871\,\mathrm{km\,s^{-1}})$. Other major clusters in this vista are the Pavo II cluster at $(\ell, b, v) = (332°\!.3 - 23°\!.6, 4167\,\mathrm{km\,s^{-1}})$, the Centaurus cluster at $(\ell, b, v) = (302°\!.4, +21°\!.6, 3418\,\mathrm{km\,s^{-1}})$, the Hydra cluster at $(\ell, b, v) = (269°\!.6, +26°\!.5, 3777\,\mathrm{km\,s^{-1}})$, and the low-latitude CIZA J1324.7−5736 and Cen–Crux clusters, at $(\ell, b, v) = (307°\!.4, +5°\!.0, 5700\,\mathrm{km\,s^{-1}})$ and $(305°, +5°, 6214\,\mathrm{km\,s^{-1}})$, respectively. The solid contour marks a line of equal Galactic foreground extinction ($A_B = 3^{\mathrm{m}}0$, from Schlegel et al. 1998).

et al. 1996; Woudt 1998). Abell et al. (1989) classified this cluster as an irregular (I) cluster with Bautz–Morgan type I (Bautz & Morgan 1970). They furthermore classify it as a richness-class 1 cluster with '59?' galaxies in the magnitude interval m_3 and $m_3 + 2$, where m_3 corresponds to the magnitude of the third brightest galaxy in the cluster. Independently, X-ray observations of the Norma cluster from *ROSAT* (Böhringer et al. 1996) and *ASCA* (Tamura et al. 1998) confirm the massive nature of this cluster. From our deep optical galaxy survey in the ZOA in the general GA region, and our follow-up redshift survey (Fairall, Woudt & Kraan-Korteweg 1998; Woudt, Kraan-Korteweg & Fairall 1999; Woudt et al. 2004), a clearer view of the obscured GA overdensity has emerged. The Norma cluster is the central cluster in a web of connected filaments and wall-like structures (Woudt 1998; Kraan-Korteweg & Lahav 2000; Radburn-Smith et al. 2006), analogous to the structures observed in and around major mass concentrations in the Λ cold dark matter (ΛCDM) Millenium Simulation (Springel et al. 2005).

One of the most prominent newly identified structures is a great-wall-like structure with the Norma cluster at its centre which we dubbed the Norma supercluster (Fairall et al. 1998; Woudt 1998), a wall of galaxies which runs nearly parallel to the Galactic plane (Kraan-Korteweg & Lahav 2000; Radburn-Smith et al. 2006) connecting the Pavo II cluster with the Norma cluster and continuing across (and nearly parallel to) the Galactic plane to the more distant Vela overdensity (Kraan-Korteweg, Fairall & Balkowski 1995) via the Cen–Crux cluster (Woudt 1998). Fig. 1 gives a clear overview of the dominant large-scale structures in the GA region.

Support for the prominence of the Norma SCL has come from various complementary multiwavelength studies at lower Galactic latitudes such as the detection of several further clusters embedded

in the Norma SCL. An X-ray search for highly obscured clusters in the ZOA (Ebeling, Mullis & Tully 2002) revealed the second most massive cluster in the Norma SCL, namely CIZA J1324.7−5736. This cluster is ~ 50–70 per cent less massive than the Norma cluster (Radburn-Smith et al. 2006) and is located at $(\ell, b, v) \sim (307°\!.4, +5°\!.0, 5700\,\mathrm{km\,s^{-1}})$. Deep near-infrared observations (Nagayama et al. 2004) furthermore uncovered a low-mass cluster around PKS 1343−601 at $(\ell, b, v) \sim (309°\!.7, +1°\!.7, 3900\,\mathrm{km\,s^{-1}})$, also within the Norma SCL. Apart from this significant collection of clusters, a general overdensity along the Norma SCL is also clearly present in the Parkes deep HI multibeam ZOA survey (Kraan-Korteweg et al. 2005).

In the first of a series of papers investigating the Norma cluster, we present a detailed dynamical analysis of this cluster, the most massive cluster in the GA overdensity, centrally located in a cosmic web of filaments and wall-like structures.

Fig. 2 shows the distribution of the optically detected galaxies (Woudt & Kraan-Korteweg 2001) in the general direction of the Norma cluster, where the Abell radius ($R_A \equiv 1.7$ arcmin/z) of the Norma cluster is indicated by the dashed circle. At the redshift of the Norma cluster (see Section 3), the Abell radius corresponds to an angular radius of $1°\!.75$. Assuming a Hubble constant of $H_0 = 73\,\mathrm{km\,s^{-1}\,Mpc^{-1}}$ and the cosmological concordance model (assumed throughout this paper), the Abell radius corresponds to a physical size of 2.0 Mpc (the cosmology-corrected angular scale at this distance is 1.16 Mpc deg^{-1}). Contours of equal Galactic foreground extinction, taken from the DIRBE/*IRAS* Galactic reddening map (Schlegel, Finkbeiner & Davis 1998), are overlaid on the galaxy distribution in Fig. 2 ($A_B = 1.0$, 1.5 and 3.0 mag, respectively; Cardelli, Clayton & Mathis 1989) and show that the Galactic
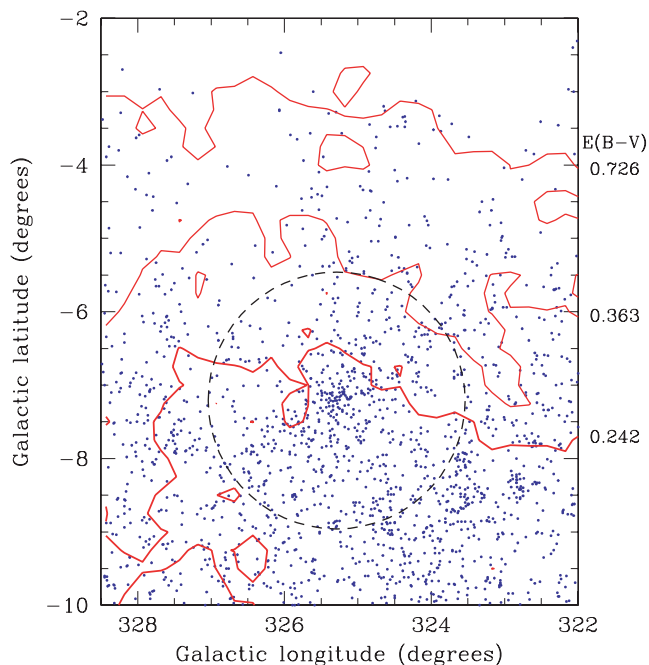
Figure 2. The distribution in Galactic coordinates of optically detected galaxies (Woudt & Kraan-Korteweg 2001) around the Norma cluster. The contours indicate lines of equal Galactic reddening (from the DIRBE/*IRAS* reddening maps, Schlegel et al. 1998) of $E(B - V) = 0.242$, 0.363 and 0.726 mag, respectively. Assuming a standard Galactic reddening law (Cardelli et al. 1989), these values correspond to $A_B = 1.0$, 1.5 and 3.0 mag, respectively. The dashed circle marks the Abell radius of the Norma cluster.

foreground extinction within the Abell radius of the Norma cluster is moderate, $A_B \leqslant 1.5$ mag.

Within the Abell radius, there are 603 optically detected galaxies with observed diameters in excess of 12 arcsec (Woudt & Kraan-Korteweg 2001) and 219 (near-infrared-detected) galaxies in the extended source catalogue (XSC) of the Two Micron All Sky Survey (2MASS, Skrutskie et al. 2006). The 2MASS galaxies in the Norma cluster represent a subset of the 603 optically detected galaxies, although not all the 2MASS galaxies have an optical counterpart; 165 of the 219 2MASS galaxies (75 per cent) were also found by Woudt & Kraan-Korteweg (2001). For the brighter 2MASS galaxies (10 arcsec aperture K_s-band < 12.5 mag), the overlap between 2MASS and the optical survey is excellent: 97 per cent of the 2MASS galaxies have an optical counterpart. It should be noted that at the position of the Norma cluster ($\ell, b \sim 325°, -7°$) star-crowding is the primary limiting factor, not the Galactic foreground extinction. The star-crowding leaves a ZOA imprint on the 2MASS XSC catalogue near the Galactic bulge (Kraan-Korteweg & Jarrett 2005) and the Norma cluster is located on the edge of this ZOA. At moderate extinction ($A_B \leqslant 3$ mag), but in the presence of severe star-crowding, optical surveys still retrieve the most complete galaxy distribution in the ZOA (Kraan-Korteweg & Jarrett 2005).

We have obtained 129 new redshifts of galaxies within the Abell radius of the Norma cluster using the 2dF spectrograph at the Anglo-Australian Observatory (AAO). These new observations are presented in Section 2. In Section 3 all the redshifts obtained to date are combined and a detailed dynamical analysis of the cluster based on 296 cluster members is presented. In Section 4, we discuss a few individual galaxies in the Norma cluster of dynamical interest.

Table 1. 2dF set-up used.

Date of observations	2001 May 30
Field centre (J2000.0)	$16^h\ 15^m\ 01\overset{s}{.}8\ -60°\ 54'24''$
Number of fibre configurations	3
Total exposure times (s)	$5 \times 1200, 5 \times 1200, 4 \times 1200$
Fibre size	2.1 arcsec ($= 0.68$ kpc at Norma)
Grating	1200V
Wavelength coverage	4700–5840 Å
Resolution (FWHM)	2.2 Å
Wavelength pixel scale	1.1 Å

2 2dF SPECTROSCOPY

Spectra were obtained with the 2dF facility (Lewis et al. 2002) on the 3.9 m Anglo-Australian Telescope. Full details of the observing 2dF set-up used for observations are given in Table 1. As the main objective was to measure the velocity dispersions of the cluster's early-type galaxies the 1200V gratings were used in each of the 2dF spectrographs. These gave a full width at half-maximum (FWHM) resolution of $\sim$125 km s^{-1} at Mg$\,b$ which is sufficient to determine velocity dispersions down to $\sim$60 km s^{-1}. In all, three fibre configurations were observed. Spectra were extracted from the raw data frames, wavelength calibrated and sky-subtracted using the AAO 2DFDR software package.[1] Redshifts were determined via cross-correlation for the absorption-line spectra and/or the direct measurement of emission lines.

The 2dF spectroscopic observations focused on the determination of accurate velocity dispersions of early-type galaxies in the Norma cluster for a Fundamental Plane analysis of the cluster. The primary target list therefore consisted of known bright ellipticals in the cluster (Woudt & Kraan-Korteweg 2001). However, we used the spare fibres of the 2dF spectrograph to extend the redshift coverage of the Norma cluster. Galaxies were primarily selected from the optical catalogue of Woudt & Kraan-Korteweg (2001) and the 2MASS XSC, indicated by 'WKK' and '2MASX J', respectively in Table 2. Additional galaxies were identified on deep R_C images taken with the ESO/MPG 2.2-m telescope and the Wide Field Imager (see Section 4). These are identified as 'ZOA J' in Table 2.

Redshifts were obtained for 182 galaxies, 53 of which had a previous measurement. For 76 galaxies, multiple measurements were obtained to gauge the internal accuracy of the 2dF spectrograph. Table 2 shows a representative sample of the results obtained from the 2dF spectroscopy. The full table is available online as Supplementary Material.

Fig. 3 shows a comparison of the measured 2dF heliocentric velocities with measurements from the literature. The vast majority of these previous measurements were obtained in the course of our ZOA redshift survey (SAAO: Woudt et al. 1999; MEFOS: Woudt et al. 2004). The overall agreement is very good:

$$v_{2dF} - v_{lit} = -6 \pm 17 \text{ km s}^{-1}$$

with a dispersion of $\sigma_{ext,all} = 124$ km s^{-1} (based on 51 galaxies). Only one galaxy revealed a discrepant heliocentric velocity; for WKK 6329, the 2dF spectroscopy resulted in $v = 4749 \pm 35$ km s^{-1} as compared to the previously low signal-to-noise ratio value for this galaxy of 2477 ± 250 km s^{-1} (Woudt et al. 1999).

[1] http://www.aao.gov.au/2df/software.html#2dfdr

Table 2. A representative sample of the results of the 2dF spectroscopy. The full table is available online as Supplementary Material.

Identification[a]	RA (2000.0)	Dec. (2000.0)	v_{abs}^b (km s^{-1})	v_{em}^b (km s^{-1})
ZOA J16070347−6113587	16 07 03.465	−61 13 58.74	15 868	
WKK 5916	16 07 50.369	−61 10 06.84	3053	
WKK 5920	16 07 52.618	−60 31 12.95	4762	
WKK 5926	16 08 08.744	−61 12 44.37		15 856
ZOA J16081355−6109377	16 08 13.548	−61 09 37.65	3640	
2MASX J16082135−6044498	16 08 21.312	−60 44 50.20	29 813	
ZOA J16083012−6039511	16 08 30.118	−60 39 51.08	6040	
WKK 5958	16 09 01.326	−60 52 03.70	15 708	
WKK 5964	16 09 06.402	−60 59 07.70	4711	
ZOA J16091138−6108285	16 09 11.377	−61 08 28.45		15 674

[a]In column 1, the WKK identification (Woudt & Kraan-Korteweg 2001) is given if the galaxy has been identified by WKK. Alternative names for galaxies are given if a WKK identification was unavailable but when the galaxy has been identified already in another survey (e.g. '2MASX J', Skrutskie et al. 2006). A new identification was given to galaxies not yet catalogued in the literature, but which we identified from deep R_C imaging (e.g. 'ZOA J', see Section 4).
[b]In columns 4 and 5, v_{abs} and v_{em} represent heliocentric velocities obtained through absorption and emission features, respectively.
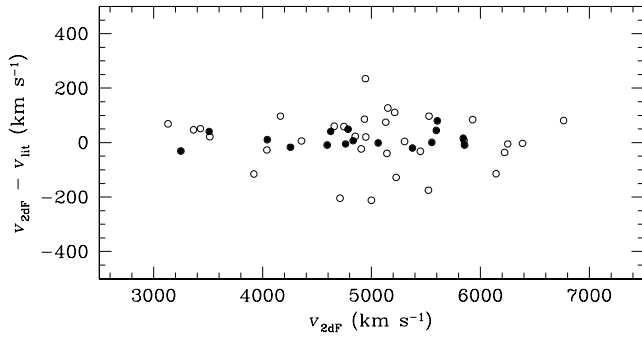
Figure 3. A comparison of the 2dF velocities with previously determined velocities.

We then compared the 2dF results with a subset of the literature sample, namely those for which redshifts were obtained with the MEFOS multifibre spectrograph (Woudt et al. 2004). This subset has the most accurate redshifts available for the Norma cluster. There are 16 galaxies in common between 2dF and MEFOS (the filled circles in Fig. 3). The agreement is again excellent, with a lower rms ($\sigma_{\rm ext,MEFOS} = 31$ km s^{-1}) than the previous comparison (which included the SAAO measurements),

$$v_{\rm 2dF} - v_{\rm MEFOS} = +12 \pm 8 \text{ km s}^{-1}.$$

Given the primary goal of obtaining accurate velocity dispersions from the 2dF spectroscopy, we have observed a large number of galaxies repeatedly to gauge the internal uncertainty: 69 galaxies were observed twice and seven galaxies had three independent velocity measurements. For these repeated observations we find $\sigma_{\rm int} = 33$ km s^{-1} over the entire range of observed velocities. This is comparable to the external comparison with the MEFOS spectroscopy. Based on these independent evaluations, we have assigned a standard error of 35 km s^{-1} to each of the 2dF velocities. The 2dF observations of the Norma cluster have resulted in the detection of 79 newly confirmed cluster members.
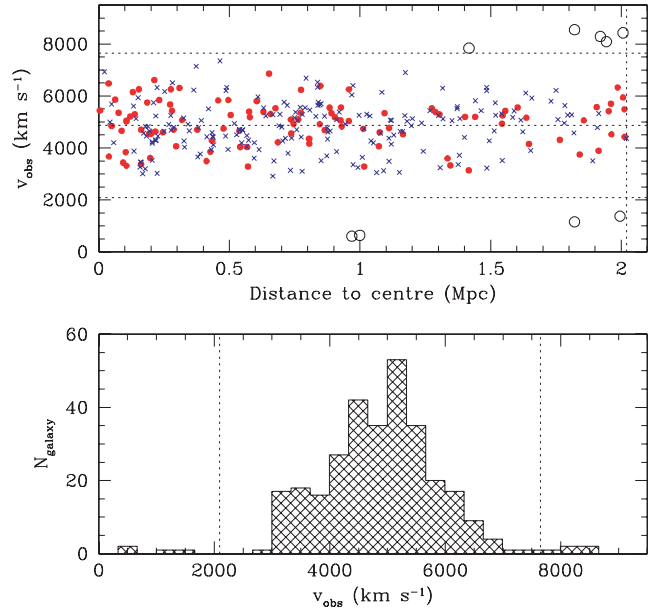
Figure 4. The upper panel shows galaxies with known redshifts as a function of distance to the central cD galaxies (WKK 6269) in the Norma cluster. The Abell radius (R_A) is indicated by the vertical dotted line, were the velocity centroid and the upper and lower 3σ limits are indicated by the horizontal dotted line. The E/S0 galaxies in the Norma cluster are plotted as filled circles and the S/Irr galaxies in the Norma cluster are shown as crosses. Galaxies deemed non-members are indicated by the open circles. The lower panel displays the velocity histogram of all galaxies within the Abell radius in the velocity range 0–9500 km s^{-1}; the upper and lower 3σ limits are marked by the vertical dashed lines.

3 DYNAMICAL ANALYSIS

3.1 Cluster membership

With the new 2dF observations described above, radial velocities are now available for 305 galaxies within the Abell radius of the Norma cluster for the velocity range 0–9500 km s^{-1}. The velocity
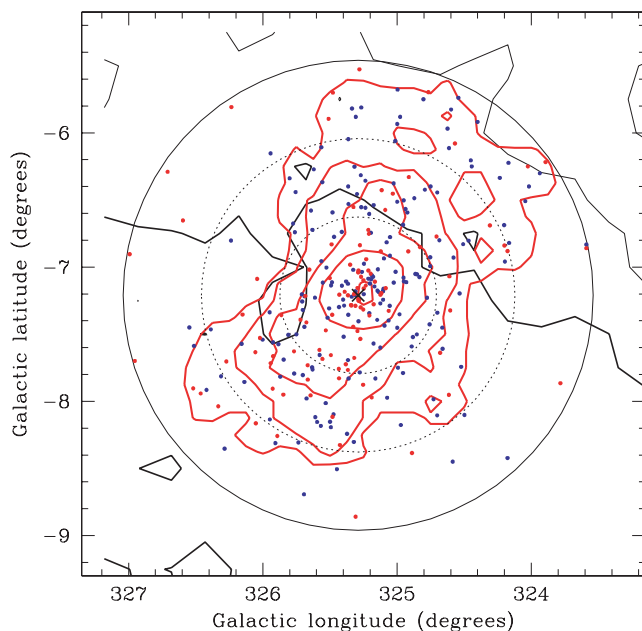
Figure 5. Galaxy density contours determined from the distribution (in Galactic coordinates) of the 296 likely cluster members. The contours have been normalized by the total number of galaxies in the sample (N_s); they correspond to 0.063 N_s, 0.125 N_s, 0.25 N_s, 0.50 N_s and 1.0 N_s galaxies per square degree, respectively. The location of WKK 6269 is indicated by the central cross, and concentric cluster radii of $(1/3)R_A$, $(2/3)R_A$ and R_A are shown as the two dashed circles and the solid circle, respectively. The extinction contours are as in Fig. 2.

distribution of these galaxies as a function of distance to the Norma cluster centre is shown in the upper panel of Fig. 4. The centre of the cluster was taken as the cD galaxy WKK 6269, a strong wide-angle-tail (WAT) radio-continuum source (Jones & McAdam 1992, 1996) located at the peak in the 0.7–10 keV *ASCA* map of the Norma cluster (fig. 1 of Tamura et al. 1998). The velocity centroid (see Section 3.2.3) of the Norma cluster is 4871 km s^{-1} and is marked by the central horizontal dashed line. The velocity limits for cluster membership are taken as ±3 times the velocity scale/dispersion (925 km s^{-1}) around the velocity centroid; these limits are shown as the upper and lower horizontal dashed line in the upper panel of Fig. 4. The ±3σ velocity limit for cluster membership is a reasonable criterion given the near-Gaussian velocity profile as shown in the lower panel of Fig. 4.

Nine galaxies are distinct outliers (open circles in the upper panel of Fig. 4) and have been rejected from our subsequent analysis. This leaves 296 likely cluster members, of which 107 have been classified as elliptical or lenticular (E/S0: filled circles in the upper panel of Fig. 4) and 189 are either spirals or irregulars (S/Irr: crosses in the upper panel of Fig. 4) (Woudt & Kraan-Korteweg 2001).

The galaxy density contours determined from the 296 cluster members, displayed in Fig. 5, show that the cluster is strongly elongated along a position angle which is aligned with the Norma wall (compare Figs 1 and 5). Since the elongation is nearly perpendicular to the Galactic extinction contours, it seems very unlikely that selective extinction effects are the cause of the observed elongation. The peak of the galaxy density distribution is located at right ascension (RA) and declination (Dec.) 16^{h}14^{m}42^s, −60°55′52″ (J2000.0), about 3 arcmin from WKK 6269 at 16^{h}15^{m}03^{s}6, −60°54′26″ (J2000.0), our adopted centre.

3.2 Substructure statistics

We employed the statistical tests described by Pinkney et al. (1993, 1996) in analysing the dynamical structure of the Norma cluster. This array of statistical tools consists of one-dimensional tests (analysing the shape of the velocity histogram), two-dimensional tests (checking for substructure in the on-sky distribution), and three-dimensional tests (using velocity and positional information). Among the latter, the Dressler–Shectman (DS) δ-test (Dressler & Shectman 1988) is a particularly powerful and frequently used method to quantify substructure (e.g. Pinkney et al. 1993; Oegerle & Hill 2001; Pimbblet, Roseboom & Doyle 2006). This test calculates the mean velocity ($\langle v \rangle_{local}$) and the standard deviation (σ_{local}) for each galaxy and its N_{nn} ($= \sqrt{N}$) nearest neighbours, where N represents the total number of galaxies in the sample; often only the 10 nearest galaxies are used in this analysis. These local parameters are then compared with the global mean ($\langle v \rangle$) and standard deviation (σ) of all the galaxies in the sample. For each galaxy, δ_i is calculated where δ_i is given by

$$\delta_i^2 = \left(\frac{N_{nn} + 1}{\sigma^2} \right) \left[(\langle v \rangle_{local} - \langle v \rangle)^2 + (\sigma_{local} - \sigma)^2 \right].$$

The cumulative deviation Δ is defined as the sum of all δ_i values. If no subclustering is present, Δ is approximately equal to the number of galaxies in the sample (N).

In the following subsections we analyse the Norma cluster at three incremental radii, starting with the inner core of the cluster ($R < 0.67$ Mpc), double this radius ($R < 1.35$ Mpc) and three times this radius out to the Abell radius ($R < 2.02$ Mpc).

3.2.1 The inner 1/3 Abell radius (= 0.67 Mpc)

Fig. 6 shows the optical image of the central 34 × 34 arcmin of the Norma cluster, obtained with the 2.2-m MPG/ESO telescope at la Silla and the Wide Field Imager during three nights in 1999 May (see also Section 4). The area displayed in Fig. 6 corresponds to ∼1.6 times the core radius (R_c; King 1966) of the Norma cluster, where $R_{c, opt} = 10.4 \pm 1.1$ arcmin (optical: Kraan-Korteweg et al. 1996) and $R_{c, X} = 9.95 \pm 1.0$ arcmin (X-ray; Böhringer et al. 1996) for the Norma cluster. In terms of the Abell radius, Fig. 6 displays the inner ∼(1/6)R_A.

Superimposed on the optical colour image are the contours of the X-ray subcluster identified by Böhringer et al. (1996) (reproduced from their fig. 2). Note that these contours mark the subcluster only and that the main cluster has been subtracted as described in Böhringer et al. (1996). The inset in Fig. 6 shows the corresponding sky distribution (in equatorial coordinates) of the identified galaxies in this field of view. The red and blue dots are confirmed cluster members, where the red dots mark E/S0 galaxies, and the blue dots correspond to S/Irr galaxies. The large black dots are galaxies (without a redshift) identified in our deep optical survey (Woudt & Kraan-Korteweg 2001) and the small black dots are galaxies (also without a redshift) identified on the deep R_C-band images taken with the Wide Field Imager. The central cD galaxy (WKK 6269, see the discussion in Section 3.4 on the peculiar velocity of this galaxy) is indicated by the black-encircled red dot.

Within $R \leqslant (1/3) R_A$, there are 129 galaxies confirmed as cluster members; 53 galaxies are E/S0 (41 per cent) and 76 have been classified as S/Irr (59 per cent), respectively. The velocity histogram of the 129 cluster members – shown in the upper panel of Fig. 7 as the cross-hatched distribution – is consistent with being Gaussian and has a biweight velocity centroid (C_{BI}) and scale (S_{BI}) (Beers,
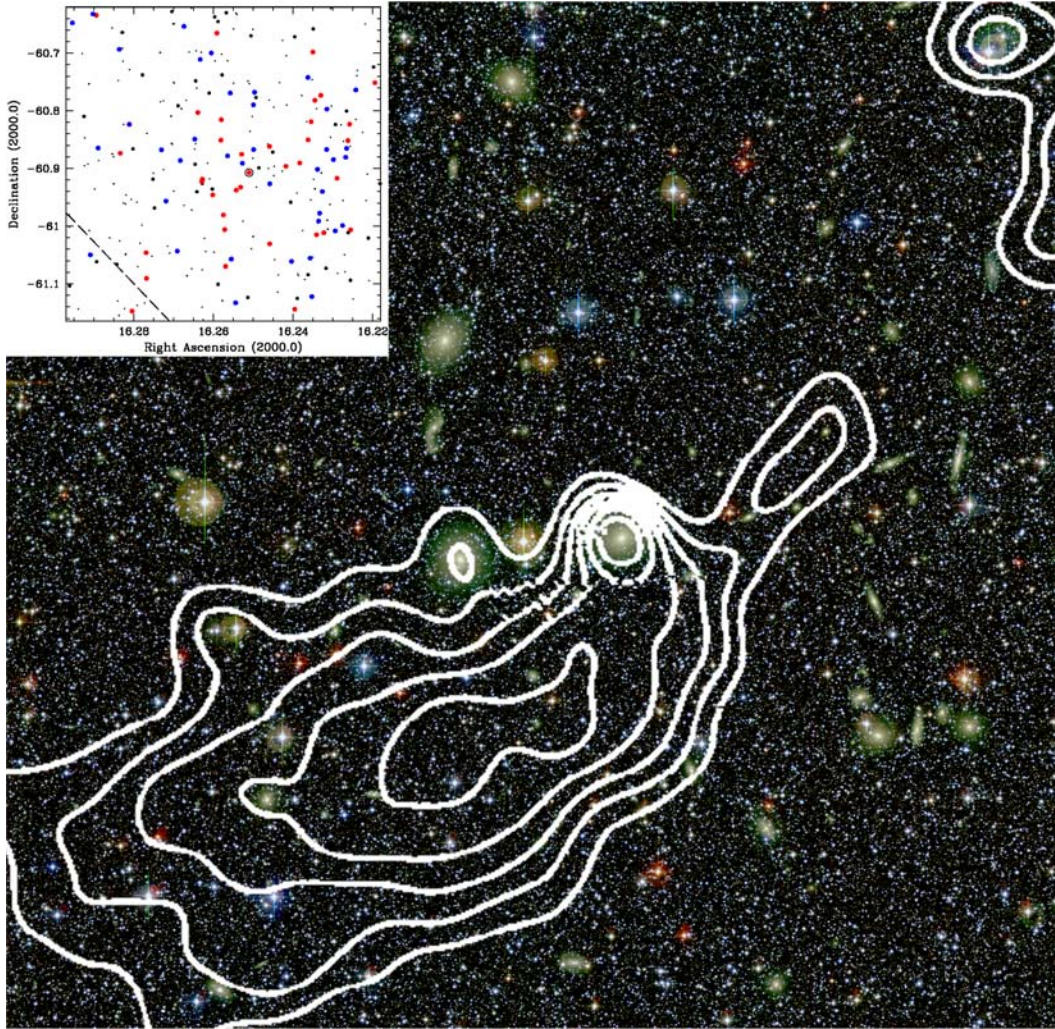
Figure 6. An optical colour image of the central $\sim 0.66 \times 0.66$ Mpc of the Norma cluster. The white contours show the X-ray subgroup identified from *ROSAT* observations (reproduced, by permission of the AAS, from Böhringer et al. 1996) overlaid on the optical galaxy distribution. The central cD galaxy (WKK 6269) coincides with the peak in the X-ray emission. The inset shows the distribution of the identified galaxies in this field of view in equatorial coordinates (E/S0 cluster members: red dots, S/Irr cluster members: blue dots, WKK galaxies with no redshift information: large black dots, small galaxies identified from the Wide Field Image data: small black dots). For reference when comparing this figure with the distribution in Galactic coordinates, a line of equal Galactic latitude ($b = -7°.5$) is drawn as a diagonal dashed line in the inset.

Flynn & Gebhardt 1990) of 4777 ± 86 and $973 \, \mathrm{km \, s^{-1}}$, respectively. When separating the sample into the elliptical and spiral population, there are some marked differences between these galaxy populations. First, the biweight velocity centroid of the two populations differ by $334 \, \mathrm{km \, s^{-1}}$ (see Table 3). The statistical significance of this difference – by analogy to the arguments used in the peculiar velocity discussion (Section 3.4) – is $S_V = 1.9$. Secondly, contrary to the velocity distribution of the elliptical galaxies (the dark shaded histogram in the top panel of Fig. 7), the velocity distribution of the spiral galaxies is non-Gaussian with hints of skewness and kurtosis.

In addition, the elliptical population is strongly elongated along a position angle in the equatorial on-sky projection of $116°$ (measured counterclockwise from north), whereas the distribution of the spiral galaxies is largely spherical. The position angle of $116°$ in equatorial coordinates corresponds to a position angle of $160°$ (measured counterclockwise from north) in the Galactic coordinate distribution at the position of the Norma cluster. The position angle of the elongated distribution is indicated by the arrows in the top left-hand

panel of Fig. 8. The location of the X-ray subcluster is indicated by the solid black line in the left-hand panels of Fig. 8. It is interesting to note the approximate alignment of the X-ray subgroup with the elongated distribution of the E/S0 galaxies. Statistical significance of the two- and three-dimensional substructure tests are calculated by means of Monte Carlo (MC) simulations (Pinkney et al. 1996). The observed sample is compared to 500 simulated samples. In the case of the elongation of the elliptical population, only four out of the 500 simulations showed a larger degree of elongation.

Despite the above mentioned differences between the elliptical and spiral galaxy population, and despite the presence of the X-ray subcluster, the DS δ-test showed no clear sign of substructure. The combined sample, as well as the E/S0 galaxy sample (and to a lesser extent the S/Irr galaxies) are formally consistent with no substructure. The Δ values for the combined sample and the individual galaxy populations are given in Table 3, together with the average value of Δ after 500 MC simulations.

Of the 500 MC simulations, 38, 75 and 14 per cent revealed a higher Δ_{MC} than the observed Δ for the combined, E/S0 and S/Irr
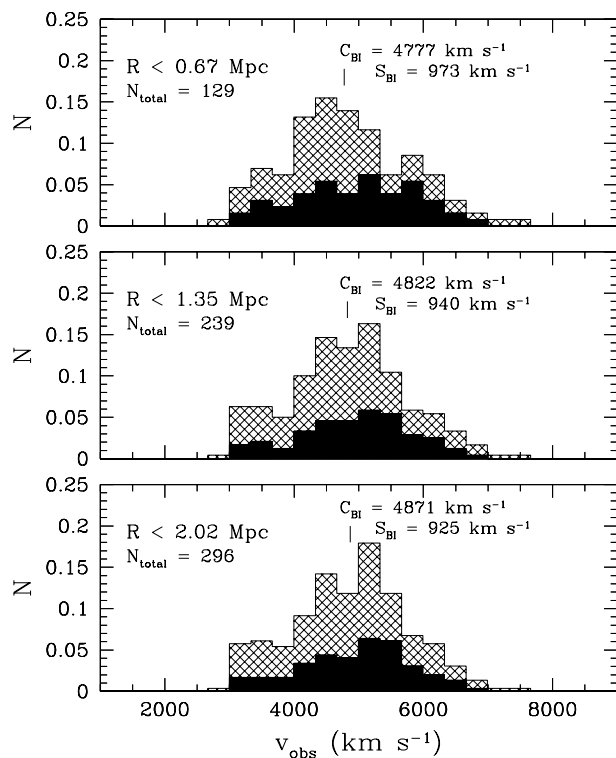
Figure 7. The normalized velocity distribution of cluster members (cross-hatched histogram) within $R < 0.67$ Mpc (upper panel), $R < 1.35$ Mpc (middle panel) and $R < 2.02$ Mpc (lower panel). In each of the panels, the velocity distribution of the E/S0 population is shown by the solid histogram.

the results of the DS δ-test for the combined sample, plotted in Galactic coordinates (as in Fig. 2). We have plotted the E/S0 galaxies (upper left-hand panel) and the S/Irr galaxies (lower left-hand panel) separately. The size of the symbols is proportional to the individual values of δ_i, where large circles indicate significant deviations from either the local mean velocity or the local mean velocity dispersion.

It should be noted that by reducing the number of nearest neighbours ($N_{nn} = 5, 7, 9$) in the DS δ-test (cf. Mohr, Geller & Wegner 1996), marginal evidence for substructure is observed for the inner 0.67 Mpc of the Norma cluster (~ 9–12 per cent of the MC simulations reveal a higher Δ_{MC}). However, the X-ray subcluster remains undetectable as a dynamically distinct subgroup.

Various individual galaxies exhibit properties which are also strongly aligned along the same position angle [WKK 6305 = PKS 1610−605: extended head–tail radio continuum emission (Jones & McAdam 1992), WKK 6176: extended X-ray tail (Sun et al. 2006)]; there is an obvious elongation within the Norma cluster which affects the way in which the galaxies interact with the intracluster medium (ICM). In Section 4 we will review some of the properties of these galaxies in more detail.

sample, respectively. Nominally, substructure is said to be present in the observed sample when less than 10 per cent of the MC simulations show a larger amount of substructure. In this case, the S/Irr galaxies reveal marginal evidence for substructure. Fig. 8 shows

3.2.2 *The inner 2/3 Abell radius (= 1.35 Mpc)*

The inner (2/3) R_A of the Norma cluster contains 239 confirmed cluster members, of which 86 are E/S0 galaxies (36 per cent) and 153 are S/Irr galaxies (64 per cent). The velocity distribution (histogram) is formally consistent with being Gaussian (see middle panel of Fig. 7), although a slight excess of spiral galaxies at lower velocities is present. The velocity centroid of the combined sample ($C_{BI} = 4822 \pm 66 \,\mathrm{km\,s^{-1}}$) is somewhat larger compared to that of the inner (1/3) R_A-sample, but this is largely due to an increase in the velocity centroid of the S/Irr population (although the velocity scale of the S/Irr galaxies has not changed). The values for the biweight velocity centroids and scales of the various samples are given in Table 3.

Table 3. An investigation into substructuring in the Norma cluster.

		$\frac{1}{3} R_A$ (= 0.67 Mpc)	$\frac{2}{3} R_A$ (= 1.35 Mpc)	$1 R_A$ (= 2.02 Mpc)
		All galaxies		
C_{BI}	(km s^{-1})	4777 ± 86	4822 ± 61	4871 ± 54
S_{BI}	(km s^{-1})	973	940	925
N		129	239	296
Δ^a		135.7 (38 per cent)	262.7 (23 per cent)	353.1 (4 per cent)
$\langle\Delta\rangle_{500}$		131.4	244.0	301.4
v_{pec} cD	(km s^{-1})	653	609	561
S_V		6.5	7.6	7.5
		Elliptical and lenticular galaxies		
C_{BI}	(km s^{-1})	4951 ± 132	4962 ± 97	4979 ± 85
S_{BI}	(km s^{-1})	964	901	877
N		53	86	107
Δ^a		44.8 (75 per cent)	83.7 (52 per cent)	107.7 (47 per cent)
$\langle\Delta\rangle_{500}$		49.6	84.4	106.9
		Spiral and irregular galaxies		
C_{BI}	(km s^{-1})	4617 ± 109	4740 ± 78	4812 ± 70
S_{BI}	(km s^{-1})	949	965	957
N		76	153	189
Δ^a		98.2 (14 per cent)	186.3 (8 per cent)	247.4 (1 per cent)
$\langle\Delta\rangle_{500}$		85.6	158.0	191.2

^{a}The percentages given after each value of Δ reflect the percentage of MC simulations which showed a higher amount of subclustering than the actual observed sample. Percentages below 10 per cent indicate significant subclustering.
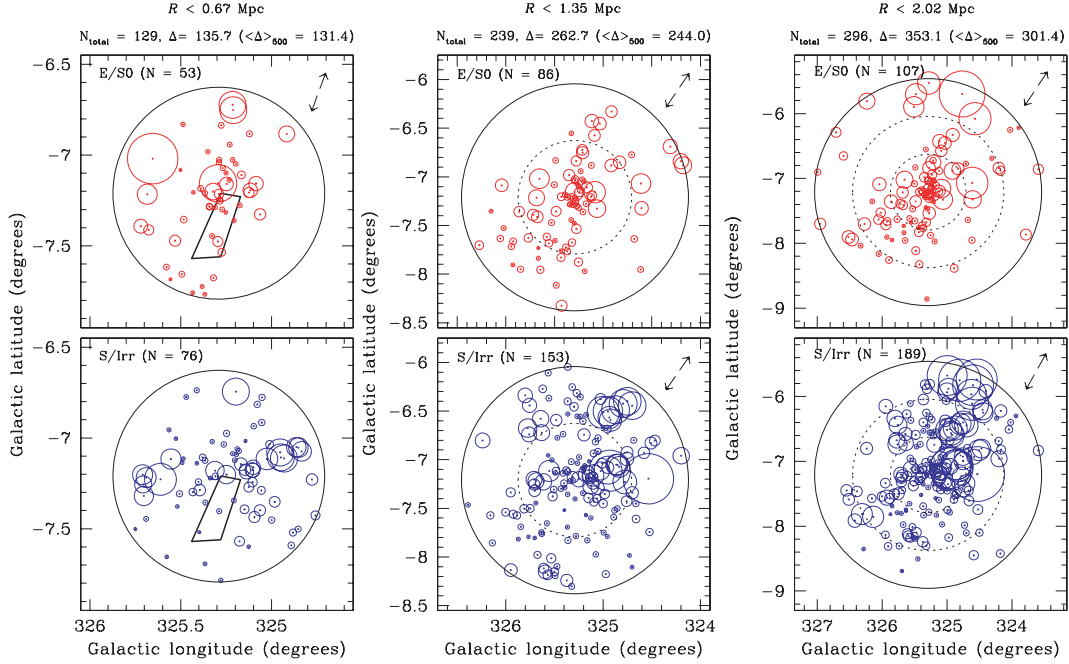
Figure 8. Results from the DS δ-test: the distribution in Galactic coordinates of galaxies and their measured δ_i. The left-hand panels show the results for the inner 0.67 Mpc (upper panel: E/S0 galaxies, lower panel: S/Irr galaxies), the middle panels show the results for the inner 1.35 Mpc (again separated by morphological classification), and the right-hand panels show the results within the entire Abell radius (2.02 Mpc). The symbol sizes are proportional to the value of e^{δ_i}, where large circles indicate significant deviations from the local mean velocity or local mean velocity dispersion. In the left-hand panels, the location of the X-ray subcluster (Böhringer et al. 1996) is marked by the solid lines. If present, the arrows in the top right-hand corner of the panels indicate the direction of the position angle of the distribution if significant elongation is detected.

The offset in the biweight velocity centroid between the E/S0 and S/Irr sample remains albeit slightly lower and is 222 km s^{-1} with a significance of $S_V = 1.8$. The velocity centroid of the E/S0 galaxies has not changed by extending the sample to a larger radius (see Table 3), although its biweight velocity scale is somewhat smaller; $S_{BI} = 901$ km s^{-1} for $R < (2/3)R_A$, compared to $S_{BI} = 964$ km s^{-1} for $R < (1/3)R_A$.

In terms of their spatial distribution, the elliptical and spiral populations now both reveal significant elongation and have position angles of 102° and 101°, respectively, in the equatorial coordinate frame. This corresponds to position angles of 146° and 145° in the Galactic coordinate frame. The latter are again indicated by arrows in the top right-hand side of the middle panels in Fig. 8. The δ-test now clearly reveals substructure in the S/Irr sample (only 8 per cent of the MC simulations show a larger degree of substructure). Interestingly, the δ-test shows that the E/S0 population is completely free of any detectable substructure. In Fig. 8, the results from the δ-test of the combined sample out to $R < 2/3 R_A$ is shown in the middle panels, where the upper middle panel shows the E/S0 galaxies and the lower middle panels displays the S/Irr galaxies.

3.2.3 The Abell radius (= 2.02 Mpc)

Our final sample extends out to the full Abell radius of the Norma cluster. Within this region, there are 296 cluster members (Section 3.1) of which 107 are classified E/S0 (36 per cent) and 189 belong to the S/Irr population (64 per cent). The velocity histogram of the combined set (the hashed histogram in the lower panel of Fig. 7) shows some evidence for kurtosis, based on the average of six kurtosis tests (Pinkney et al. 1996), and a clear excess of galaxies at lower velocities. The difference in the velocity centroid of

the two morphologically distinct samples is reduced to 167 km s^{-1} (164 km s^{-1} in the cluster rest frame) at a significance of $S_V = 1.5$.

The spatial distribution of both the E/S0 galaxies and the S/Irr galaxies is strongly elongated with position angles of 102° and 107°, respectively, in the equatorial coordinate frame. This corresponds to 146° and 151° in the Galactic coordinate reference frame; these angles are indicated by the arrows in the top right-hand corner of the right-hand panels in Fig. 8. The uncertainty in the position angle is ∼7°.

As before, the E/S0 population appears relaxed. Their velocity centroid remains constant throughout the cluster (4979 ± 85 km s^{-1} for all the E/S0 galaxies within the Abell radius) and no substructure is detected by the DS δ-test. The velocity scale (S_{BI}) of the E/S0 sample shows a distinct decrease as a function of radius (see Table 3), again a signature of a relaxed rich cluster (Rines et al. 2003).

The spiral galaxy population, on the other hand, appears far from relaxed. The velocity centroid increases with increasing radius (shifting by ∼200 km s^{-1} across the Abell radius) and the velocity scale stays roughly constant at ∼960 km s^{-1}. The MC simulations of the DS δ-test of the S/Irr galaxies indicate that only 1 per cent of the simulations show a larger degree of substructure compared to the observed amount of substructure. The results of the δ-test of the combined sample ($N = 296$) is shown in the right-hand panels of Fig. 8.

3.3 Subgroups in the Norma cluster

We have identified two spiral-rich subgroups based on the DS δ-test of the S/Irr population alone. When displaying those S/Irr galaxies for which $\delta_i > 2.25$, two distinct groups appear. In Fig. 9 the distribution in Galactic coordinates of the 296 cluster members are
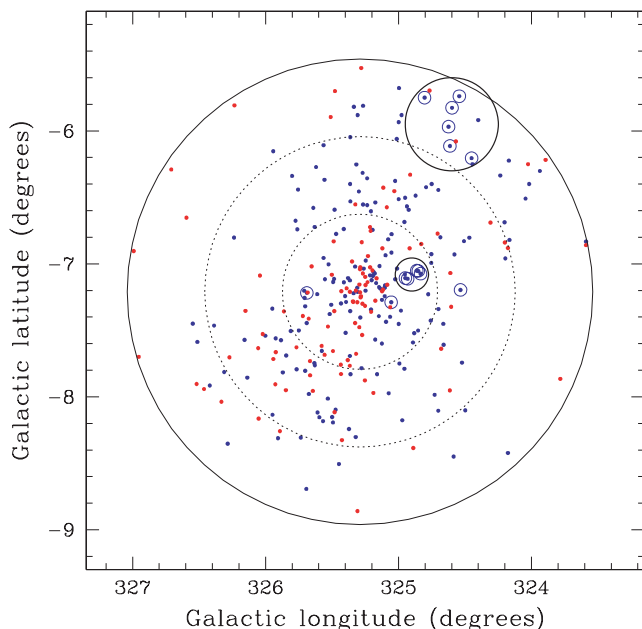
Figure 9. The distribution in Galactic coordinates of the 296 cluster members within the Abell radius. Encircled dots represent spiral galaxies with $\delta_i \geqslant 2.25$ (based on the δ-test of the entire S/Irr galaxy population). Two spiral-rich subgroups have been identified and are marked by the solid circles.

shown, where spiral galaxies with $\delta_i > 2.25$ are shown as encircled dots. This δ_i limit was chosen based on the outcome of the δ-test of the E/S0 galaxies; that sample is completely free of any substructure and there the largest measured δ_i was 2.25. A few isolated galaxies also appear with large δ_i values.

In the case of WKK 6406 at $(\ell, b, v) = (325°69, -7°22, 7349 \pm 35 \, \text{km s}^{-1})$, its large heliocentric velocity could indicate that it is a background galaxy which was mistakenly identified as a cluster member (see also the upper panel of Fig. 4).

Close to the centre of the Norma cluster is a compact group (dubbed 'Norma A') where we have isolated a group of five dynamically distinct galaxies around WKK 6078 (including WKK 6071, WKK 6078, WKK 6125, WKK 6135 and ZOA J16113352). This group is marked in Fig. 9 by the small solid circle within the $R < (1/3) R_A$ region (inner dashed circle). The centre of Norma A is approximately at RA and Dec. $16^h12^m00^s, -61°04'40''$ (J2000.0). Based on these five galaxies, we find a mean velocity of $4453 \, \text{km s}^{-1}$ (which is $418 \, \text{km s}^{-1}$ less than the mean of the cluster, corresponding to $411 \, \text{km s}^{-1}$ in the cluster rest frame). Norma A has a velocity dispersion of $312 \, \text{km s}^{-1}$, which is much smaller than the velocity scale of the cluster ($925 \, \text{km s}^{-1}$).

A second dynamically distinct group of galaxies ('Norma B') is found further from the core of the cluster, centred around WKK 5751 (other galaxies include WKK 5718, WKK 5779, WKK 5783, WKK 5796 and WKK 5813). This group is indicated by the large solid circle in Fig. 9 in the region $\frac{2}{3}R_A < R < R_A$ and has a central position (in RA and Dec.) of $16^h03^m56^s, -60°26'54''$ (J2000.0). It has a mean velocity of $5313 \, \text{km s}^{-1}$ (an offset of $+435 \, \text{km s}^{-1}$ in the cluster rest frame) and a velocity dispersion of $604 \, \text{km s}^{-1}$.

Norma B (and to a lesser extent Norma A) lies along the Norma wall elongation, supporting the idea that cluster infall occurs along the connecting filaments and wall-like structures. This is consistent with the large-scale structure formation and evolution as seen in the

ΛCDM Millenium Simulation (Springel et al. 2005). To gauge how far the merger of both Norma A and B with the main cluster (Norma major) has progressed, deep observations with the Australian Telescope Compact Array (ATCA) could be used to determine whether the spiral galaxies in Norma A and Norma B are hydrogen-deficient as a result of interactions with the ICM. Previous observations with ATCA of the Norma cluster (Vollmer et al. 2001) showed that spirals in the Norma cluster are generally H I-deficient, but these observations did not include Norma A and B, respectively.

3.4 The peculiar velocity of the central cD galaxy

The Norma cluster contains two large cD galaxies, namely WKK 6312 at $v_{cD} = 3839 \pm 38 \, \text{km s}^{-1}$ (Woudt et al. 2004) and WKK 6269 at $v_{cD} = 5441 \pm 52 \, \text{km s}^{-1}$ (Woudt et al. 2004). The latter has been observed with the 2dF and was found to be in excellent agreement with previous measurements: $v_{cD} = 5448 \pm 35 \, \text{km s}^{-1}$, see Table 2). WKK 6269 is also known as PKS B1610−608 (one of the 20 strongest extragalactic radio sources) and is a textbook example of a WAT radio galaxy (Jones & McAdam 1992, 1996). Such WAT morphology either reflects the motion of the cD galaxy through the cluster and its interaction with the ICM via ram pressure (Owen & Rudnick 1976), or indicates the presence of a cluster–subcluster merger (Burns 1998).

Whether WKK 6269 is at rest with respect to the potential well of the cluster can be assessed from its peculiar velocity, i.e. the difference between the velocity centroid of the cluster (C_{BI}) and the velocity of the individual cD galaxy (v_{cD}). The peculiar velocity has to be corrected by a factor $(1 + z)$ to ensure the velocity difference is in the cluster rest frame and considered independently for the varying values in the three regarded spheres.

In Table 3 we also list the values of the peculiar velocity of WKK 6269 as determined within the various spheres. It ranges from $\sim 650 \, \text{km s}^{-1}$ within a radius of 0.67 Mpc to $\sim 550 \, \text{km s}^{-1}$ within 2.02 Mpc. The statistical significance of this peculiar velocity ranges from 6.5 to 7.5 ($S_V \equiv |v_{cD} - C_{BI}|/\sqrt{\sigma_1^2 + \sigma_2^2}$, where σ_1 is the error in the velocity centroid of the cluster and σ_2 is the error in the velocity measurement of the cD galaxy). The large number of cluster members used to determine the velocity centroid ($\sigma_1 = S_{BI}/\sqrt{N_{gal}}$) and the small error in the measurement of the heliocentric velocity of WKK 6269, makes this large peculiar velocity highly significant. It is exceptionally large when compared to other cD galaxies in clusters (Oegerle & Hill 2001), but not without precedent (Pimbblet et al. 2006; Andernach et al. 2007). Note that the other cD galaxy in the Norma cluster (WKK 6312) has an even larger velocity offset.

Böhringer et al. (1996) identified an X-ray subgroup close the centre of the Norma cluster (see Fig. 6). This subgroup (dubbed 'Norma minor') is fairly massive; Tamura et al. (1998) estimate that the mass of this subgroup could add up to ~ 50 per cent to the total mass of the cluster.

A comparison of the 843-MHz radio continuum emission of PKS B1610−608 (Jones & McAdam 1992) with the X-ray contours of this central subgroup (shown in Fig. 11) shows that the radio lobes of WKK 6269 are closely aligned with the X-ray subgroup. The large observed peculiar velocity of the cD galaxy in the Norma cluster is most likely caused by this ongoing merger.

Based on the compactness of the X-ray subcluster, Böhringer et al. (1996) argued that the merger has not progressed very far yet, and that most of the main component of the cluster is still undisturbed by the collision. This is consistent with simulations of cluster mergers (Pinkney et al. 1996), which show that large peculiar velocities can

Table 4. Mass estimates of the Norma cluster.

X-ray mass (gravitational)		
R (h_{73}^{-1} Mpc)[a]	$M(<R)$ (h_{73}^{-1} M$_\odot$)[a]	Reference
0.68	1.5–4.0×10^{14}	Böhringer et al. (1996)
0.75	3×10^{14}	Tamura et al. (1998)
2.05	2.9–15×10^{14}	Böhringer et al. (1996)
	Dynamical mass	
R (h_{73}^{-1} Mpc)	$M(<R)$ (h_{73}^{-1} M$_\odot$)	
all galaxies	$M_{\rm VT}$	$M_{\rm RVT}$	$M_{\rm PME}$
0.67	4.2×10^{14}	4.3×10^{14}	6.6×10^{14}
1.35	8.1×10^{14}	8.6×10^{14}	11.6×10^{14}
2.02	10.4×10^{14}	11.0×10^{14}	14.7×10^{14}

[a]The original values have been converted from h_{50}^{-1} to h_{73}^{-1}.

be reproduced in the event of large-scale mergers at the time of core-crossing. If this merger takes place close to the plane of the sky, it would also explain the non-results of the statistical tests. These are least sensitive to mergers occurring perpendicular to the line of sight. Therefore, the X-ray morphology – in combination with the large peculiar motion of the central cD galaxy – strongly suggests a recent or commencing merger at the core of the cluster.

3.5 Dynamical mass estimate

For the determination of the dynamical mass of the Norma cluster, we have used both the virial theorem ($M_{\rm VT}$) and the projected mass estimator ($M_{\rm PME}$), see equations (21) and (22) of Pinkney et al. (1996). The use of the biweight velocity centroid and scale (Beers et al. 1990) in the virial theorem (instead of the velocity mean and standard deviation) leads to a more robust mass estimate ($M_{\rm RVT}$). The latter is more robust against the effects of contamination by the inclusion of possible non-members in the analysis. The projected mass estimator (Bird 1995), on the other hand, is sensitive to the presence of (spatially separated) subclusters due to its proportionality to the projected distance between galaxy i and the cluster centroid ($R_{\perp,i}$) (see equation 22 in Pinkney et al. 1996). The presence of a spatially separated subcluster (e.g. in a pre-merger configuration) would result in a systematic offset with respect to the cluster centroid; this leads to larger values of $R_{\perp,i}$ and thus to a significantly larger mass estimate. For a full discussion of the appropriate use of these dynamical mass estimators we refer to Pinkney et al. (1996) and Bird (1995).

The three dynamical mass estimates ($M_{\rm VT}$, $M_{\rm RVT}$ and $M_{\rm PME}$) determined within the three radial limits (using the combined samples of $N = 129$, 239 and 296 galaxies, respectively) are given in Table 4. On average, $M_{\rm RVT}$ is ~5 per cent larger than $M_{\rm VT}$. The projected mass estimate, however, is generally about 50 per cent larger than $M_{\rm VT}$ and indicates the presence of a spatially distinct subcluster (projected on the plane of the sky) presumably in the early stages of merging (Pinkney et al. 1996). This is consistent with our previous indications of subclustering, particularly in the form of Norma minor (the X-ray subgroup).

Böhringer et al. (1996) and Tamura et al. (1998) both give an estimate of the gravitational mass of the Norma cluster based on *ROSAT* and *ASCA* X-ray observations, respectively. In Table 4, we list the values (converted from h_{50}^{-1} to h_{73}^{-1}) of the mass within a specific radius as derived from X-ray observations by Böhringer et al. (1996) and Tamura et al. (1998). Both virial mass estimates ($M_{\rm VT}$ and $M_{\rm RVT}$) are consistent with the mass determined from the
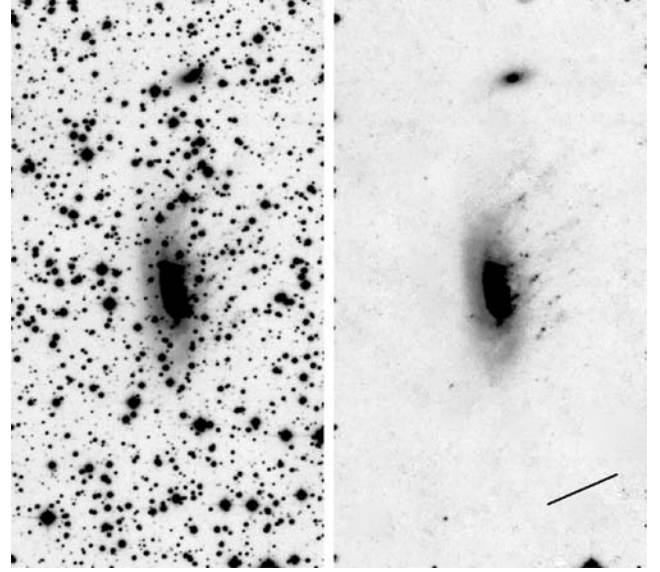

Figure 10. The R_C-band image of WKK6176 before (left-hand panel) and after star subtraction (right-hand panel) using the KILLALL routine (Buta & McCall 1999) in IRAF. The field of view is 2.2×4.0 arcmin^2, north is up and east is to the left-hand side. The diagonal bar at the bottom right-hand side in the star-subtracted image indicates the position angle of the elongated E/S0 population within $R < 0.67$ Mpc.

X-ray luminosity of the cluster. In the presence of substantial sub-clustering, as suggested here for the Norma cluster, all dynamical mass estimators could still overestimate the true mass of the cluster, depending on the projection angle of the cluster–subcluster merger axis with respect to the line of sight (Pinkney et al. 1996). This effect is smallest for $M_{\rm VT}$ and $M_{\rm RVT}$ for a merger occurring perpendicular to the line of sight. We can therefore safely conclude that the mass of the Norma cluster within the Abell radius corresponds to 1–$1.1 \times 10^{15}\, h_{73}^{-1}$ M$_\odot$. This confirms the status of the Norma cluster as the most massive cluster in the GA.

4 INDIVIDUAL GALAXIES

A number of galaxies in the Norma cluster show direct or indirect evidence of interaction with the ICM. Here, we will explore these galaxies in some detail in the light of the preceding discussion.

4.1 WKK 6176 and the X-ray tail

Recent *Chandra* and *XMM–Newton* observations of WKK 6176 (= ESO 137−001) revealed the presence of a ~70 kpc long X-ray tail pointing away from the cluster centre (Sun et al. 2006), suggesting this galaxy is undergoing a significant amount of gas stripping. The extent of this X-ray tail is unusual (Sun et al. 2006).

We have deep *B*-, *V*- and R_C-band photometry of WKK 6176. These data were obtained in 1999 May with the MPG/ESO 2.2-m telescope at la Silla and the Wide Field Imager (ESO Programme 63.N-0054). We covered the entire Abell radius of the Norma cluster for the purpose of measuring the R_C-band luminosity function (see also Fig. 6). This optical as well as the near-infrared J, H and K_s luminosity function of the Norma cluster will be presented in a separate paper in this series.

WKK 6176 is located close to the core of the Norma cluster. In Fig. 6 it can be found at (RA, Dec.) ~ ($16\overset{h}{.}224\,25$, $-60\overset{\circ}{.}763\,97$), to the lower left-hand side of the rightmost X-ray contours (aligned

Table 5. Selected galaxies in the Norma cluster.

Galaxy	Observational characteristic	Position angle (°)
WKK 6176	70 kpc X-ray tail	129
	Optical filaments	125
WKK 6269[a]	Central cD galaxy	128
WKK 6305	500 kpc radio-continuum tail	108

[a]The position angle quoted here for WKK 6269 is a mean position angle as determined from GALFIT (Peng et al. 2002) isophotal fitting of deep K_s-band imaging.

with the virtual extension of the X-ray subgroup). A close-up of WKK 6176 is shown in Fig. 10 where we have displayed the R_C-band image in a field of view of 2.2×4.0 arcmin. Given the low Galactic latitude of the Norma cluster ($b \sim -7°$) and proximity to the Galactic bulge (only $35°$ away), a large number of stars are superimposed on the galaxy images. Reliable photometry can only be obtained after careful removal of the many foreground stars. We used the KILLALL routine developed by Buta & McCall (1999) within the IRAF [2] environment to remove this stellar contamination. Fig. 10 illustrates the effectiveness of this star-removal procedure for the Norma cluster galaxy WKK 6176 (compare the right-hand panel of Fig. 10 to the original image). It also reveals numerous striking low-brightness filaments to the west of WKK 6176, appearing to stream away from WKK 6176 at a position angle of $\sim 125°$. Several bright knots (distinctly different from the Galactic foreground pollution) appear within these filaments. The low surface brightness filaments are aligned with the X-ray tail (Sun et al. 2006), but are not only confined to the region of the X-ray tail. For comparison, we have indicated the direction of the major axis of the E/S0 galaxy population with the diagonal marker in Fig. 10.

WKK 6176 is a low-redshift equivalent of the two recently detected spiral galaxies in massive rich clusters (Abell 2667 and Abell 1689) at $z \sim 0.2$ which show clear evidence for galaxy transformation (Cortese et al. 2007). Interestingly, WKK 6176 is located at a similar projected distance from the centre of the Norma cluster (0.28 Mpc) as the two high-redshift spirals in Abell 2667 and Abell 1689, which lie at $0.34\,h_{70}^{-1}$ Mpc and $0.24\,h_{70}^{-1}$ Mpc from their respective cluster centre.

A full investigation into the properties of WKK 6176 as derived from multiwavelength photometry (BVR_CJHK_s), spectroscopy, and galaxy evolution modelling (Fritze-v. & Woudt 2006), and its implications for galaxy evolution in dense environments will be presented elsewhere.

4.2 WKK 6305: the head–tail radio continuum source

Another peculiar galaxy in the Norma cluster is WKK 6305, also known as PKS 1610−605 (Jones & McAdam 1996). It is located at a similar distance from the centre of the cluster (0.29 Mpc) as WKK 6176. In Fig. 11 we show an overview of the central region with the same field of view as Fig. 6. The galaxy distribution of confirmed cluster members and the X-ray subgroup are as before, but now the radio continuum emission of WKK 6269 and WKK 6305 at 843 MHz are overplotted (reproduced from Jones & McAdam 1992). WKK 6305 corresponds to the head–tail source visible in
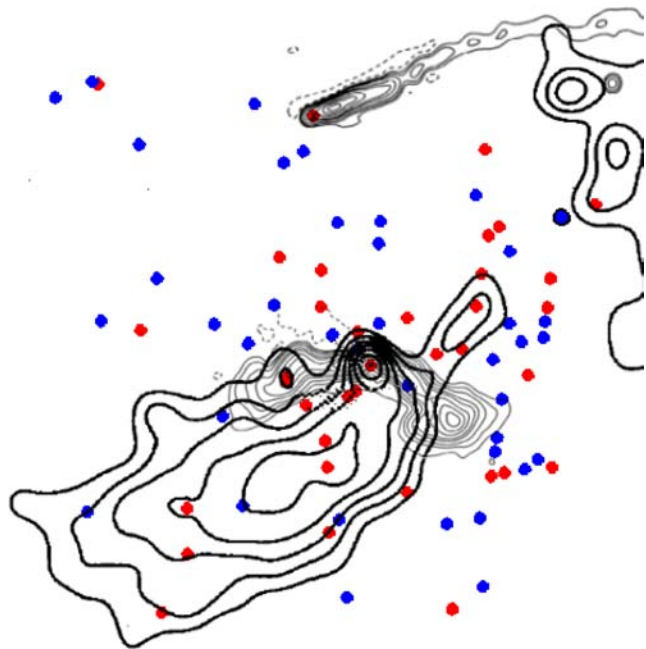
[2] IRAF is distributed by the National Optical Astronomy Observatories, which are operated by the Association of Universities for Research in Astronomy, Inc., under cooperative agreement with the National Science Foundation.

Figure 11. The galaxy distribution and the X-ray subgroup of the inner $\sim 0.66 \times 0.66$ Mpc (as in Fig. 6; reproduced, by permission of the AAS, from Böhringer et al. 1996) with the radio continuum emission (reproduced, by permission of the AAS, from Jones & McAdam 1992) of WKK 6269 and WKK 6305 overplotted. WKK 6176 is indicated by the large dot in the virtual extension of the X-ray subgroup.

Fig. 11. The tail length of 26 arcmin (~ 500 kpc at the distance of the Norma cluster) represents one of the longest radio continuum tails observed. The position angle of the tail is $\sim 108°$ (Jones & McAdam 1996) and is, as before with the X-ray tail of WKK 6176, closely aligned with the elongated (E/S0) galaxy distribution in the cluster.

5 DISCUSSION

The dynamical analysis of the Norma cluster presented here has revealed a significant amount of subclustering in this nearby rich cluster, ranging from the central X-ray group to the two spiral-rich subgroups further from the core of the cluster. Even though the X-ray group did not show up in the dynamical analysis, the large peculiar velocity of the cD galaxy, whose radio lobes appear to 'embrace' the X-ray contours of this central group, is a tell-tale sign of an ongoing merger. The large discrepancy between M_{PME} and the mass determined from the virial theorem (where $M_{MPE} \sim 1.5 \times M_{VT}$) is an independent indication of the presence of a spatially separated subcluster of substantial mass. Significant subclustering is not unusual for rich and massive clusters; Colless & Dunn (1996) in their detailed dynamical analysis of the archetypical rich Coma cluster also revealed the presence of an ongoing merger.

The galaxy distribution in the Norma cluster is clearly elongated, with a position angle (in equatorial coordinates) ranging between $116°$ (for the central part) and $\sim 105°$ (for the overall distribution). It should be emphasized that this observed elongation is not an artefact of selective Galactic extinction effects at this low Galactic latitude. The position angle of the major axis of the Norma cluster, as indicated by the arrows in Fig. 8, runs nearly perpendicular to the lines of constant Galactic foreground extinction (compare with

Fig. 2). The elongated galaxy distribution is aligned with the major large-scale structure in this region as can be seen in Fig. 1. Such an alignment is not unexpected within the cluster-rich GA environment (Binggeli 1982).

Within the cluster itself, various galaxies show clear evidence for interactions with the ICM. An overview of these galaxies and their defining characteristics is given in Table 5. The defining features of these galaxies are strongly aligned with the general galaxy distribution of the cluster. In the case of WKK 6176 and WKK 6305, they are X-ray/optical and radio continuum tails, respectively, whereas for WKK 6269 (the central cD galaxy) the major axis of the galaxy is aligned with the cluster (see Table 5).

6 CONCLUSION

The Norma cluster (ACO 3627) is a nearby, rich and massive cluster – on par with the more distant Coma cluster – which resides at the bottom of the potential well of the GA. The galaxy distribution of the cluster members shows a clear elongation which is aligned with the main wall-like structures of the GA. Despite the relaxed appearance of the early-type galaxy population in the Norma cluster, a large amount of subclustering is present. We have identified two spiral-rich subclusters (Norma A and B) in addition to the previously identified central (X-ray) subcluster (Norma minor). The ongoing merger of the latter with the main cluster (Norma major) is assumed to be responsible for the large peculiar motion of the central cD galaxy.

The proximity of the Norma cluster offers an excellent opportunity to study the interaction of cluster members such as WKK 6176 with the ICM at high resolution and sensitivity.

REFERENCES

Andernach H., Alamo-Martínez K., Coziol R., Tago E., 2007, in Saviane I., Ivanov V., Borissova J., eds, ESO Astrophysics Symposia, Groups of Galaxies in the Nearby Universe. Springer-Verlag, Berlin, p. 395
Abell G. O., Corwin H. G., Olowin R. P., 1989, ApJS, 70, 1
Bautz L. P., Morgan W. W., 1970, ApJ, 162, L149
Beers T. C., Flynn K., Gebhardt K., 1990, AJ, 100, 32
Binggeli B., 1982, A&A, 107, 338
Bird C. M., 1995, ApJ, 445, L81
Böhringer H., Neumann D. M., Schindler S., Kraan-Korteweg R. C., 1996, ApJ, 467, 168
Burns J. O., 1998, Sci, 280, 40
Buta R. J., McCall M. L., 1999, ApJS, 124, 33
Cardelli J. A., Clayton G. C., Mathis J. S., 1989, ApJ, 345, 245
Colless M., Dunn A. M., 1996, ApJ, 458, 435
Cortese L. et al., 2007, MNRAS, 376, 157
Dekel A., 1994, ARA&A, 32, 371
Dressler A., 1988, ApJ, 329, 519
Dressler A., Shectman S. A., 1988, AJ, 95, 985

Dressler A., Faber S. M., Burstein D., Davies R. L., Lynden-Bell D., Terlevich R. J., Wegner G., 1987, ApJ, 313, 37
Ebeling H., Mullis C. R., Tully R. B., 2002, ApJ, 580, 774
Einasto M., Tago E., Jaaniste J., Einasto J., Andernach H., 1997, A&AS, 123, 119
Erdoğdu P. et al., 2006, MNRAS, 373, 45
Fairall A. P., Woudt P. A., Kraan-Korteweg R. C., 1998, A&AS, 127, 463
Fritze-v. Alvensleben U., Woudt P. A., 2006, in Whitelock P. A., Dennefeld M., Leibundgut B., eds, Proc. IAU Symp. 232, Scientific Requirements for Extremely Large Telescopes. Cambridge University Press, Cambridge, p. 223
Hudson M. J., 1993a, MNRAS, 265, 43
Hudson M. J., 1993b, MNRAS, 265, 72
Hudson M. J., Smith R. J., Lucey J., Branchini E., 2004, MNRAS, 352, 61
Jahoda K., Mushotzky R. F., 1989, ApJ, 346, 638
Jones P. A., McAdam W. B., 1992, ApJS, 80, 137
Jones P. A., McAdam W. B., 1996, MNRAS, 282, 137
King I., 1966, AJ, 71, 64
Kocevski D. D., Ebeling H., 2006, ApJ, 645, 1043
Kolatt T., Dekel A., Lahav O., 1995, MNRAS, 275, 797
Kraan-Korteweg R. C., Jarrett T., 2005, in Fairall A. P., Woudt P. A., eds, ASP Conf. Ser. Vol. 329, Nearby Large-Scale Structures and the Zone of Avoidance. Astron. Soc. Pac., San Francisco, p. 119
Kraan-Korteweg R. C., Lahav O., 2000, A&AR, 10, 211
Kraan-Korteweg R. C., Fairall A. P., Balkowski C., 1995, A&A, 297, 617
Kraan-Korteweg R. C., Woudt P. A., Cayatte V., Fairall A. P., Balkowski C., Henning P. A., 1996, Nat, 379, 519
Kraan-Korteweg R. C., Staveley-Smith L., Donley J., Koribalski B., Henning P. A., 2005, in Colless M., ed., Proc. IAU Symp. 216, Maps of the Cosmos. Astron. Soc. Pac., San Francisco, p. 203
Lewis I. J. et al., 2002, MNRAS, 333, 279
Lucey J., Radburn-Smith D., Hudson M. J., 2005, in Fairall A. P., Woudt P. A., eds, ASP Conf. Ser. Vol. 329, Nearby Large-Scale Structures and the Zone of Avoidance. Astron. Soc. Pac., San Francisco, p. 21
Lynden-Bell D., Lahav O., 1988, in Rubin V. C., Coyne G. V., eds, Large-Scale Motions in the Universe. Princeton University Press, Princeton, NJ, p. 199
Lynden-Bell D., Faber S. M., Burstein D., Davies R. L., Dressler A., Terlevich R. J., Wegner G., 1988, ApJ, 326, 19
Mohr J. J., Geller M. J., Wegner G., 1996, AJ, 112, 1816
Nagayama T. et al., 2004, MNRAS, 354, 980
Oegerle W. R., Hill J. M., 2001, AJ, 122, 2858
Owen F. N., Rudnick L., 1976, ApJ, 205, 1
Peng C. Y., Ho L. C., Impey C. D., Rix H.-W., 2002, AJ, 124, 266
Pimbblet K. A., Roseboom I. G., Doyle M. T., 2006, MNRAS, 368, 651
Pinkney J., Rhee G., Burns J. O., Hill J. M., Oegerle W., Batuski D., Hintzen P., 1993, ApJ, 416, 36
Pinkney J., Roettiger K., Burns J. O., Bird C. M., 1996, ApJS, 104, 1
Proust D. et al., 2006, A&A, 447, 133
Radburn-Smith D. J., Lucey J. R., Woudt P. A., Kraan-Korteweg R. C., Watson F. G., 2006, MNRAS, 369, 1131
Rines K., Geller M. J., Kurtz M. J., Diaferio A., 2003, AJ, 126, 2152
Rowan-Robinson M. et al., 1990, MNRAS, 247, 1
Scaramella R., Baiesi-Pillastrini G., Chincarini G., Vettolani G., Zamorani G., 1989, Nat, 338, 562
Schlegel E. M., Finkbeiner D. P., Davis M., 1998, ApJ, 500, 525
Skrutskie M. F. et al., 2006, AJ, 131, 1163
Springel V. et al., 2005, Nat, 435, 629
Sun M., Jones C., Forman W., Nulsen P. E. J., Donahue M., Voigt G. M., 2006, ApJ, 637, L81
Tamura T., Fukazawa Y., Kaneda H., Makishima K., Tashiro M., Tanaka Y., Böhringer H., 1998, PASJ, 50, 195
Tonry J. L., Blakeslee J. P., Ajhar E. A., Dressler A., 2000, ApJ, 530, 625
Vollmer B., Cayatte V., van Driel W., Henning P. A., Kraan-Korteweg R. C., Balkowski C., Woudt P. A., Duschl W. J., 2001, A&A, 369, 432
Woudt P. A., 1998, PhD thesis, Univ. Cape Town

Woudt P. A., Kraan-Korteweg R. C., 2001, A&A, 380, 441

Woudt P. A., Kraan-Korteweg R. C., Fairall A. P., 1999, A&A, 352, 39

Woudt P. A., Kraan-Korteweg R. C., Cayatte V., Balkowski C., Felenbok P., 2004, A&A, 415, 9

SUPPLEMENTARY MATERIAL

The following supplementary material is available for this article.

Table 2. Results of the 2dF spectroscopy.

This material is available as part of the online article from: http://www.blackwell-synergy.com/doi/abs/10.1111/j.1365-2966. 2007.12571.x (this link will take you to the article abstract).

Please note: Blackwell Publishing are not responsible for the content or functionality of any supplementary materials supplied by the authors. Any queries (other than missing material) should be directed to the corresponding author for the article.

This paper has been typeset from a TEX/LATEX file prepared by the author.